Self-Alignment of Dye Molecules in Micelles and Lamellae for Three-Dimensional Imaging of Lyotropic Liquid Crystals

Qingkun Liu,[†,‡,§] Corinne Beier,[†] Julian Evans,[†,‡] Taewoo Lee,[†,‡] Sailing He,[§,‖] and Ivan I. Smalyukh[*,†,‡,⊥]

[†]Department of Physics, University of Colorado, Boulder, Colorado 80309, United States
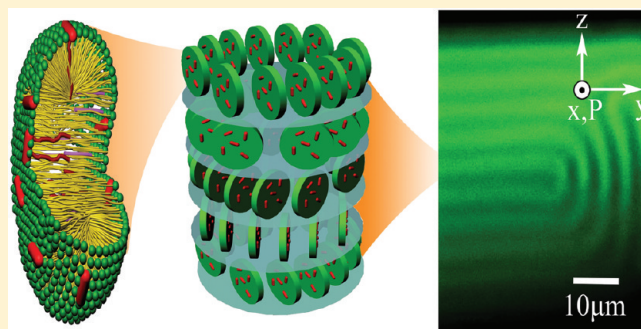
[‡]Liquid Crystal Materials Research Center, University of Colorado, Boulder, Colorado 80309, United States

[§]Centre for Optical and Electromagnetic Research, Zhejiang University, Hangzhou 310058, People's Republic of China

[‖]Department of Electromagnetic Engineering, Royal Institute of Technology, S-100 44 Stockholm, Sweden

[⊥]Renewable and Sustainable Energy Institute, National Renewable Energy Laboratory and University of Colorado, Boulder, Colorado 80309, United States

ABSTRACT: We report alignment of anisotropic amphiphilic dye molecules within oblate and prolate anisotropic micelles and lamellae, the basic building blocks of surfactant-based lyotropic liquid crystals. Absorption and fluorescence transition dipole moments of these dye molecules orient either parallel or orthogonal to the liquid crystal director. This alignment enables three-dimensional visualization of director structures and defects in different lyotropic mesophases by means of fluorescence confocal polarizing microscopy and two-photon excitation fluorescence polarizing microscopy. The studied structures include nematic tactoids, Schlieren texture with disclinations in the calamitic nematic phase, oily streaks in the lamellar phase, developable domains in the columnar hexagonal phase, and various types of line defects in the discotic cholesteric phase. Orientational three-dimensional imaging of structures in the lyotropic cholesterics reveals large Burgers vector dislocations in cholesteric layering with singular disclinations in the dislocation cores that are not common for their thermotropic counterparts.

1. INTRODUCTION

Liquid crystals (LCs) are a classic example of soft materials, typically possessing long-range orientational order combined with varying degrees of partial positional order and chirality.[1,2] The simplest type of LCs, the so-called nematic liquid crystals, are comprised of self-aligned anisotropic molecules or multi-molecular building blocks whose local average orientation is described by the director with nonpolar symmetry $\mathbf{n}(\mathbf{r}) \equiv -\mathbf{n}(\mathbf{r})$. This orientational ordering is supplemented by unidirectional twist in the ground-state structures of the cholesteric phase, by quasi-long-range one-dimensional positional order in the lamellar phase and by two-dimensional positional order in the columnar phase. LCs have both fundamental and technological importance and are also of profound interest from the biological standpoint because of the liquid crystalline behavior exhibited by lipids, viruses, biopolymers, and membranes.[3-5] The elasticity- and defect-mediated interactions between incorporated colloidal particles in LCs are markedly different from those in isotropic media, allowing for novel means of nanoscale and microscale colloidal self-assembly that have attracted a great deal of recent interest.[6-10] Columnar hexagonal, lamellar, and other lyotropic mesophases are frequently used as templates to obtain mesoporous silica structures.[11]

A remarkable and technologically useful property of the thermotropic LCs is that they can align small dye molecules of size comparable to that of LC molecules (this is the well-known guest–host effect)[2] and also nanometer-sized and much bigger micrometer-sized colloidal particles, forcing these foreign inclusions to follow the spatial patterns of orientational order and director structures of LCs. Alignment of anisotropic colloidal particles (such as gold nanorods) in surfactant-based lyotropic LCs has also been achieved.[12] However, long-range ordering of small anisotropic molecules comparable to the size of surfactant molecules and much smaller than the self-organized micelles is presently a challenge. This precludes a number of potential applications that require such alignment (i.e., lyotropic cholesteric LC distributed-feedback lasers) and the use of this alignment for orientation-sensitive fluorescence imaging purposes.[3,13,14]

Fluorescence confocal microscopy and multiphoton excitation fluorescence microscopy are broadly used to study three-dimensional (3D) composition morphology and structural properties of biological and soft matter systems,[13] including LCs. Furthermore, by using anisotropic fluorescent dye molecules along with polarized excitation and fluorescence detection, one can visualize 3D patterns of $\mathbf{n}(\mathbf{r})$ in an approach called fluorescence confocal polarizing
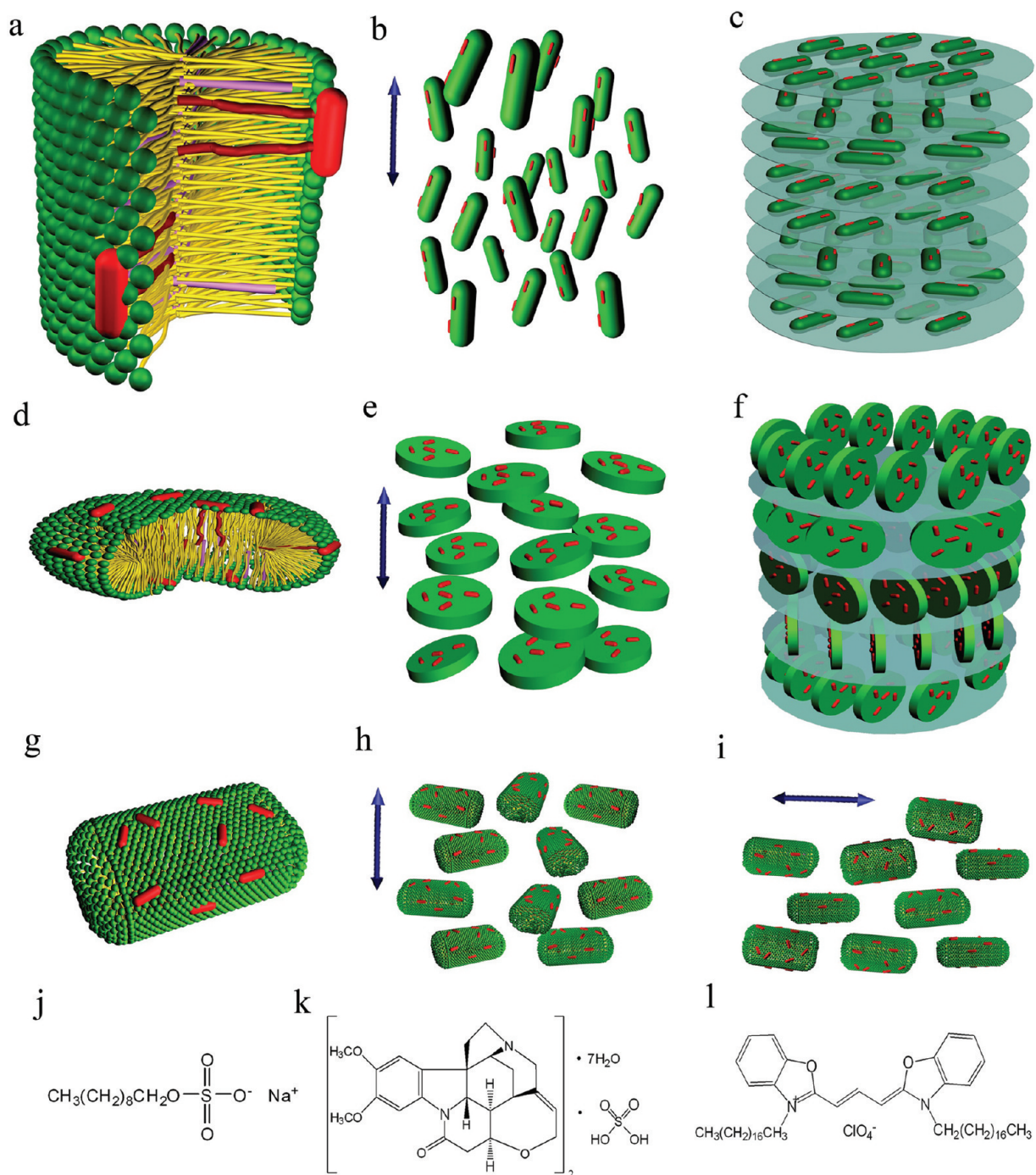
Figure 1. Alignment of amphiphilic dye molecules in the calamitic and discotic micelles. (a) A schematic of the self-oriented $DiOC_{18}(3)$ dye molecules (red) having anisotropic aromatic cores along the axis of a cylindrical SDS/1-decanol micelle. (b) A schematic of alignment of the dye molecules along $\mathbf{n}(\mathbf{r})$ in the calamitic nematic phase. (c) A schematic of alignment of the dye molecules along $\mathbf{n}(\mathbf{r})$ in the cholesteric phase formed by the cylindrical micelles. (d) A schematic of the oriented self-assembly of $DiOC_{18}(3)$ dye molecules (red) in a discoid SDS/1-decanol micelle (note that the hydrocarbon chains of the dye molecule are about 2 times longer than those of SDS). (e) A schematic of alignment of the dye molecules in the discotic nematic phase. (f) A schematic of alignment of the dye molecules in the cholesteric phase formed by the discoid micelles. (g) The orthorhombic micelles of nematic liquid crystals originate the different nematic phases by different orientational fluctuations, giving rise to (h) discotic nematic phase and (i) calamitic nematic phase. Molecular structures of (j) the amphiphilic molecule of sodium decyl sulfate (SDS), (k) chiral agent molecule of brucine sulfate heptahydrate, and (l) the dye molecule of $DiOC_{18}(3)$. We note that the schematics a–i represent highly idealized models of micelles and their self-organization into mesomorphic structures; however, the micelles in the real lyotropic systems have rather imperfect geometric shapes, and the alignment of used dye molecules is also much less perfect than what is depicted on the schematics.

microscopy (FCPM).[13−19] In this approach, the absorption and fluorescence transition dipoles of the dye molecules spontaneously follow $\mathbf{n}(\mathbf{r})$ while the dye molecules homogeneously distributes within the LC sample. Two-photon excitation fluorescence

polarizing microscopy (2PEFPM) works in a similar way but excites the dye molecules through the two-photon absorption process using a pulsed laser beam and provides images with higher spatial resolution with a stronger sensitivity to the molecular orientations patterns.[16–18] By use of linearly polarized excitation and fluorescence detection, the FCPM and 2PEFPM techniques yield 3D patterns of fluorescence intensity that visualize the 3D structures of $\mathbf{n(r)}$.[14–18] Furthermore, 2PEFPM is capable of dynamic imaging of various fast processes related to field-induced transformation of 3D director fields in thermotropic liquid crystals.[20] The rodlike fluorescent probe dyes are commonly employed to visualize $\mathbf{n(r)}$ of thermotropic LCs by detecting the polarized fluorescence of probe dyes aligned along the director and parallel to the calamitic LC molecules. Dye intercalation between the base pairs of DNA has been utilized to probe the patterns of molecular alignment in lyotropic LCs composed of DNA bio-polymers.[19,21] However, FCPM and 2PEFPM imaging of liquid crystalline materials composed of complex multimolecular building blocks, such as anisotropic surfactant micelles, is challenging and has not been previously demonstrated. To accomplish this, one needs fluorescent dye molecules capable of localizing within such molecular building blocks and exhibiting appropriate alignment. In biological systems, such as phospholipid membranes, the orientation of fluorescent dye molecules and their diffusion and rotational dynamics have been extensively explored in recent studies.[22–27] However, the distinct orientation of small dyes in anisotropic self-assembled structures such as those of highly anisotropic micelles and its use for visualization of $\mathbf{n(r)}$ of lyotropic LCs made of these micelles have not been explored.

In this work, we demonstrate that dye molecules having rodlike rigid aromatic cores and the hydrocarbon tails self-assemble into the prolate cylindrical surfactant micelles and self-align with their absorption and fluorescence transition dipole moments parallel to the surfactant micelle's long axis and along $\mathbf{n(r)}$. These dye molecules also self-assemble into the oblate discoid surfactant micelles and lamellae and self-align parallel to the surfactant layers but show random ordering within them; their alignment in this case is perpendicular to $\mathbf{n(r)}$ of these mesophases. This self-alignment of the dye molecules allows for 3D imaging of the director field and defects of the lyotropic LC materials in different mesomorphic phases by means of both FCPM and 2PEFPM techniques. The demonstrated application of these 3D imaging techniques to the study of surfactant-based lyotropic systems allows for direct nondestructive high-resolution visualization of LC director field in arbitrary cross-sectional planes of a selected 3D volume of a lyotropic LC sample that has not been achieved before. We show that these imaging approaches can be successfully utilized in the study of all major types of lyotropic mesophases, including those possessing orientational ordering only as well as orientational order accompanied by either chirality or partial one-dimensional or two-dimensional positional ordering.

2. EXPERIMENTAL SECTION

We studied the ternary lyotropic LC system of sodium decyl sulfate–decanol–water (SDS/1-decanol/water, Figure 1) with a well-established phase diagram.[28,29] This system allows us to obtain a number of different mesomorphic phases comprised of building blocks such as cylindrical and disk-shaped micelles and lamellae. Typically, the LC in the calamitic nematic phase (Figure 1b) was prepared using a composition of 36 wt % of SDS (Figure 1j), 7 wt % of 1-decanol (both from

Sigma-Aldrich, used as supplied), and 57 wt % of deionized water. Deionized water was obtained from the Barnstead/Thermolyne E-pure system (>17 Mohm·cm). As the mixing and sample conditions were varied, a biphasic system was obtained in certain parts of the sample with droplets (tactoids) of nematic composed of calamitic micelles. Thorough mixing of the components of this ternary system was followed by ultrasonication for 2 h at room temperature. To obtain the LC in a discotic cholesteric phase (Figure 1f), 1.1 mol % of the chiral agent brucine sulfate heptahydrate (BSH, obtained from Sigma-Aldrich) (Figure 1k) was added to the discotic nematic preparation of 36.5 wt % of SDS, 6.5 wt % of 1-decanol, and 57 wt % of deionized water to obtain an equilibrium pitch p of about 10 μm. The lyotropic LC in the columnar phase was prepared as above nematic-phase samples but consisted of 45 wt % SDS, 3 wt % 1-decanol, and 52 wt % of deionized water which organized in a two-dimensional packing of cylindrical micelles in a hexagonal lattice. The lyotropic LC in the lamellar phase was prepared as above but consisted of 28 wt % SDS, 8 wt % 1-decanol, and 64 wt % of deionized water. In addition, 0.01 wt % of the fluorescent dye $DiOC_{18}(3)$ (3,3'-dioctadecyloxacarbocyanine perchlorate, obtained from Invitrogen, chemical structure shown in Figure 1l) was added into these samples for the 3D fluorescence imaging purposes.

The FCPM setup is assembled on the base of a Olympus FV 300 laser scanning confocal microscope with an achromatic linear polarization rotator. The excitation beam (488 nm, Ar-ion laser) is focused by an objective into a small (<1 μm^3) volume in the sample cell. The fluorescent light from this volume is detected by a photomultiplier tube in the spectral region of 510–550 nm selected by interference filters. The use of a pinhole in the detection channel (located in a plane confocal with the focal plane of the objective) of the fluorescence confocal microscope allows one to achieve submicrometer resolution along the optical axis of the microscope, in addition to the similar diffraction-limited resolution in the lateral plane of the FCPM microscope. The 2PEFPM imaging is performed by excitation with a 980 nm femtosecond pulse from a tunable (680–1080 nm) Ti:sapphire oscillator (140 fs, 80 MHz, Chameleon Ultra-II, Coherent) and by forward detection with various interference filters used to separate the fluorescent light from the excitation laser beam.[17,18] This nonlinear optical process of two-photon absorption of the dye molecules attains better resolution in both axial and radial directions as well as a stronger sensitivity to molecular orientations.[17,18] Simultaneously with the FCPM and 2PEFPM imaging, transmission-mode polarizing microscopy (PM) textures of the same sample are recorded by measuring the intensity of light that passes through a polarizer, sample, and an analyzer oriented orthogonally to the polarizer.

3. RESULTS AND DISCUSSION

3.1. Self-Alignment of Dye Molecules Decorating the Spatial Patterns of n(r). The cationic amphiphilic fluorescent chromophore $DiOC_{18}(3)$ is widely used as a lipophilic tracer of cell membranes and readily incorporates into surfactant mono-layers and bilayers (Figure 1).[13] Its two long hydrocarbon chains are on the same side of the rodlike aromatic part of the chromophore (Figure 1l). When used as a membrane dye, the two carbocyanines of the $DiOC_{18}(3)$ molecules localize at the aqueous interface region of the membranes. Conjugated carbocyanines of this molecule have absorption/fluorescence transition dipole moments oriented parallel to the aromatic part of the chromophore, which enables direct molecular orientation study of the chromophore in membranes by means of polarized excitation and fluorescence detection.

Figure 1 shows the schematic representation of $DiOC_{18}(3)$ molecules incorporated into different types of micelles. When
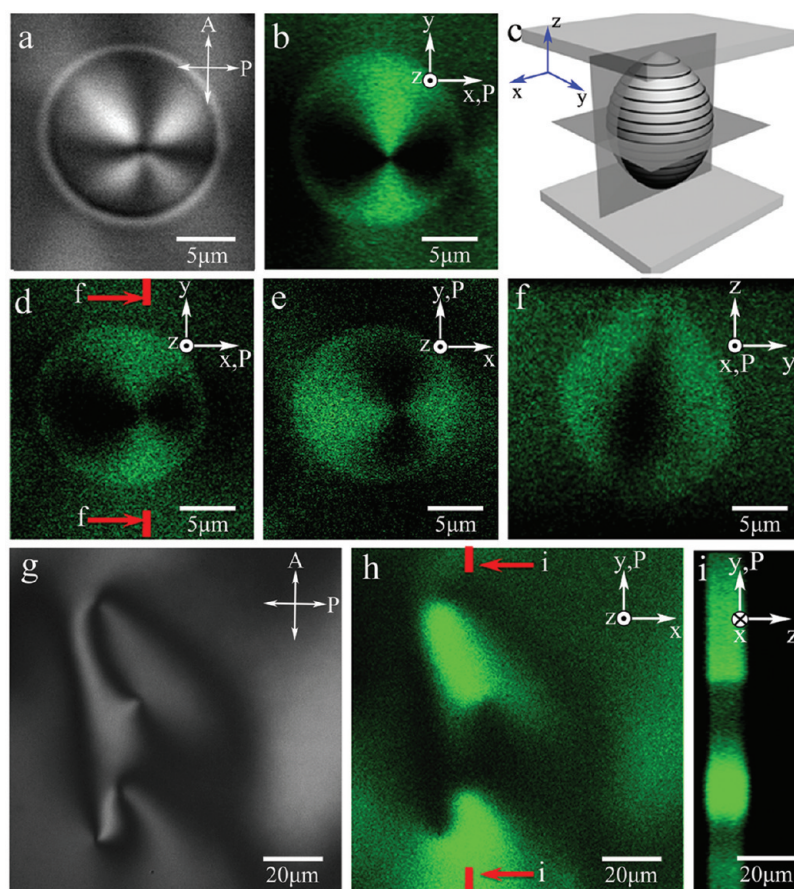
Figure 2. Comparative 3D imaging and analysis of nematic director structures formed by cylindrical micelles by means of PM, 2PEFPM, and FCPM techniques. (a) PM and (b) 2PEFPM cross-section images in the cell midplane of a nematic tactoid, a biphasic system with droplets of nematic composed of calamitic micelles surrounded by an isotropic surrounding, confined between two glass plates, as schematically shown in (c); the black concentric lines in (c) depict $\mathbf{n(r)}$. Similar FCPM images obtained for (d, e) in-plane cross section with two orthogonal polarizations $\mathbf{P}$ of probing light (as marked on the images) and (f) vertical cross section of the sample. (g) PM and (h, i) FCPM images of $\mathbf{n(r)}$ structures and defects in the calamitic lyotropic nematic phase obtained for both (h) in-plane xy and (i) vertical yz cross section, as marked on the images. The red lines in (d) and (h) indicate locations where the cross sections (f) and (i) are taken. Crossed polarizer "$\mathbf{P}$" and analyzer "$\mathbf{A}$" are marked in (a, g).

intercalating into the highly curved structure of a cylindrical micelle (Figure 1a), the rodlike rigid aromatic part of the dye molecule aligns along the micelle to fit its structure without locally disrupting the intrinsic curvature, while the hydrocarbon tails of the dye (about 2 times longer than that of the used surfactant molecules) span across the micelle. Because the surface of cylindrical micelles with the diameter of about 2.6 nm is highly curved compared with the size of rodlike rigid aromatic part of the dye molecule (which is about 1.3 nm in length), the alignment is robust and observed in different studied mesophases formed by these micelles (nematic, cholesteric, and columnar hexagonal).[30] According to many of the literature studies, the size of the micelle in calamitic nematic phase is about 2.6 nm in diameter and 6.0 nm long while the size of the micelle in the discotic nematic phase is about 5.7 nm in diameter and 2.0 nm in thickness.[30] Another model (based on the profile of the X-ray diffraction bands obtained in the nematic phases of potassium laurate/decanal/water ternary system) suggests that, at least in some of the lyotropic systems, the micelles might have orthorhombic shapes; the typical dimensions of the micelle estimated within the framework of this model are 8.5 nm by 5.5 nm in the plane perpendicular to the bilayer with the thickness of the bilayer being 2.6 nm (Figure 1g).[29,31,32] In addition to the curvature-induced orientational alignment and hydrophobic–hydrophilic

interactions that cause incorporation of the dye molecules into micelles, an important role might be played by electrostatic interactions between the charged molecules composing these building blocks of the lyotropic LC and the charged dye molecules (the details and interplay of different types of interactions are of great interest and will be explored and discussed in detail elsewhere).

The alignment of the dye molecules leads to the transition dipole moments of absorption and fluorescence of the dye following the local orientations of micelles and the mesoscopic spatial patterns of $\mathbf{n(r)}$, as schematically demonstrated for the examples of the ground-state nematic and cholesteric structures shown in Figure 1b,c. When introduced into the same ternary system in a lamellar phase, or in a nematic phase formed by disk-shaped micelles, the amphiphilic molecules of $DiOC_{18}(3)$ intercalate into the flat bilayers or prolate micelles of the surfactant molecules so that their rodlike aromatic parts of molecules and absorption/fluorescence transition dipoles are parallel to the planes of lamellae or prolate micelle but show random ordering within them (Figure 1d–f). By detecting the polarization-dependent fluorescence of chromophore molecules, the collinear orientation of transition dipoles of fluorescence and absorption of the chromophore can be determined and used to reconstruct the 3D patterns of $\mathbf{n(r)}$. In the case of the model of orthorhombic
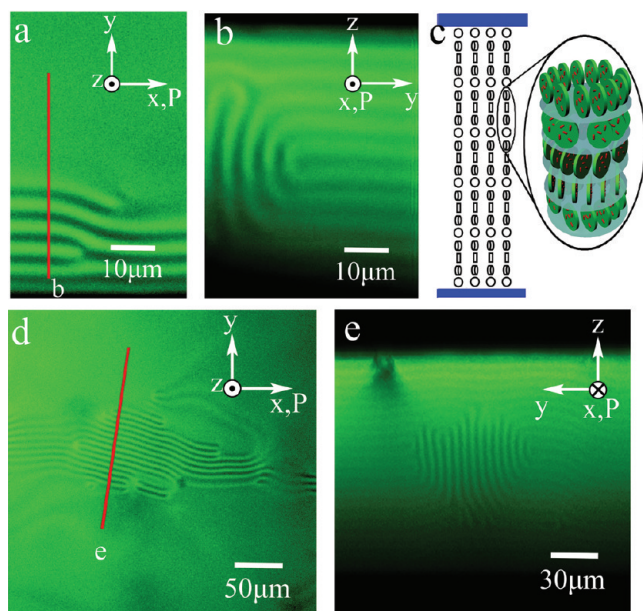
Figure 3. FCPM 3D imaging of $\mathbf{n(r)}$ structures and defects in lyotropic cholesteric LCs formed by discoid micelles using $DiOC_{18}(3)$ as a fluorescent probe. (a) In-plane image of the lyotropic cholesteric LC with regions having both lateral and vertical orientation of layers and dislocations. (b) Vertical cross section along the red line marked in (a), in which 3D layers' distortions and dislocations are clearly visualized. (c) Schematic representation of $\mathbf{n(r)}$ of the planar structure of the cholesteric LC in the right-side part of the cross section shown in (b). The discs schematically represent many micelles changing their orientation continually; there are about 2000 micellar disks along the z-axis in each stripe, with the bilayer planes being parallel to the helical axis. (d) FCPM image of a lyotropic cholesteric LC with strongly distorted layered pattern and several types of dislocations visible in the lateral xy plane. (e) Vertical cross sections obtained along red line labeled in (d) reveal 3D layered patterns, $\mathbf{n(r)}$, and defects in the unaligned lyotropic cholesteric LC sample. The used polarization of FCPM is marked by "$\mathbf{P}$" on the images.

micelles of the surfactant-based nematic LCs, orientational fluctuations of micelles that predetermine the symmetry axis of the phase, perpendicular to the largest micellar surface, give rise to the average orientation of transition dipoles of fluorescence and absorption of the chromophores perpendicular to the director of discotic nematic LC (Figure 1h). The orientational fluctuations that define the symmetry axis in the plane of the largest micellar surface, along the longest axis of the flattened ellipsoid, give rise to the average orientation of transition dipoles of fluorescence and absorption of the chromophore parallel to the director of the uniaxial calamtic nematic LC (Figure 1i). Therefore, $\mathbf{n(r)}$ can also be reconstructed by use of the polarization-dependent fluorescence of the chromophore. However, in the case of possible biaxial nematic phases, one would need to utilize more than one type of dye in order to elucidate the 3D structures of different directors of biaxial nematic LCs.

3.2. Three-Dimensional Imaging of Director Fields and Defects. Well-defined alignment of anisotropic amphiphilic dye molecules with respect to the anisotropic building blocks of lyotropic LCs allows for high-contrast 3D imaging of $\mathbf{n(r)}$ and defects by use of FCPM and 2PEFPM. Figure 2 shows images of the $\mathbf{n(r)}$ structures and defects in nematic tactoids formed by cylindrical micelles. The tactoidal nematic droplet touches the two opposite glass plates of the sample cell and shows
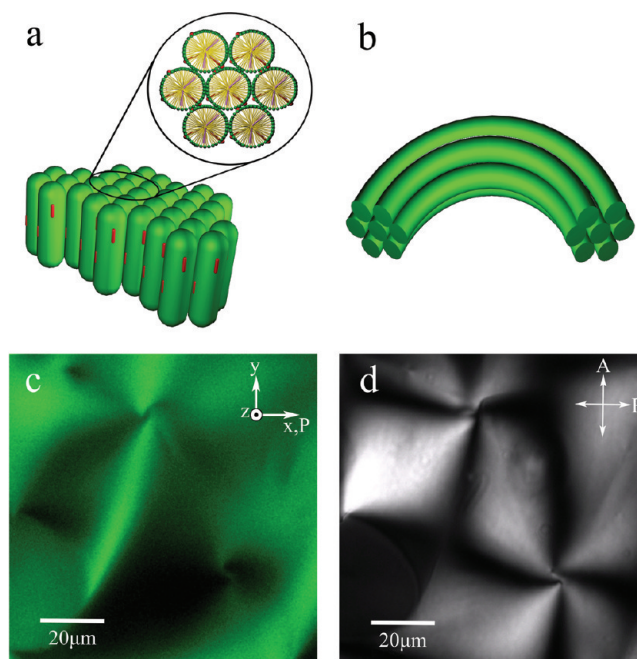

Figure 4. FCPM and PM imaging of $\mathbf{n(r)}$ in the lyotropic columnar hexagonal LC with developable domains. (a) Schematic representation of the self-assembly of cylindrical micelles with the aligned $DiOC_{18}(3)$ dye molecules incorporated into them in the columnar hexagonal phase. (b) A schematic of bend-type distortions of the columnar structure of cylindrical micelles within the developable domains. Collocated (c) FCPM and (d) PM images of the columnar LC sample areas that allow one to visualize developable domains and corresponding bend-type distortions of $\mathbf{n(r)}$. The polarization of the FCPM probing light is marked by "$\mathbf{P}$" in (c), and the crossed polarizer "$\mathbf{P}$" and analyzer "$\mathbf{A}$" are marked in (d).

polarization-dependent fluorescence textures (Figure 2b−f). The analysis of the images obtained in both FCPM and 2PEFPM modes and at different polarizations of probing light reveals the toroidal director structure with a twist-escaped +1 nonsingular disclination inside the nematic tactoid running across the cell and along the tactoid's diameter (Figure 2a−f), as schematically shown in Figure 2c. The FCPM images obtained for the ternary lyotropic system fully in a nematic phase are shown in Figure 2h,i and reveal four half-integer singular disclinations (two of strength −1/2 and two of strength +1/2) running across the LC cell. The FCPM and 2PEFPM images are consistent with the corresponding PM texture shown in Figure 2a,g (note that the PM textures have been obtained by use of the monochromatic laser light in a transmission mode). We note that the demonstrated mapping of $\mathbf{n(r)}$ in the plane perpendicular to the LC cell would be impossible by means of conventional imaging techniques such as optical polarizing microscopy, for both nematic and biphasic parts of the phase diagram.

Figure 3 shows FCPM images of an unaligned lyotropic cholesteric LC in both lateral and vertical cross sections of the sample, allowing one to visualize the details of 3D layered patterns and defects in this system. This cholesteric sample is composed of disk-shaped micelles forming a cholesteric structure schematically shown in Figure 1f and has the dye molecules with transition dipole moments parallel to the large-area faces of the micelles. The bright and dark stripes visualize the layered cholesteric structure [one lamella of half-pitch $(p/2)$ thickness is equivalent to the twist of $\mathbf{n(r)}$ by π] in the sample, with the
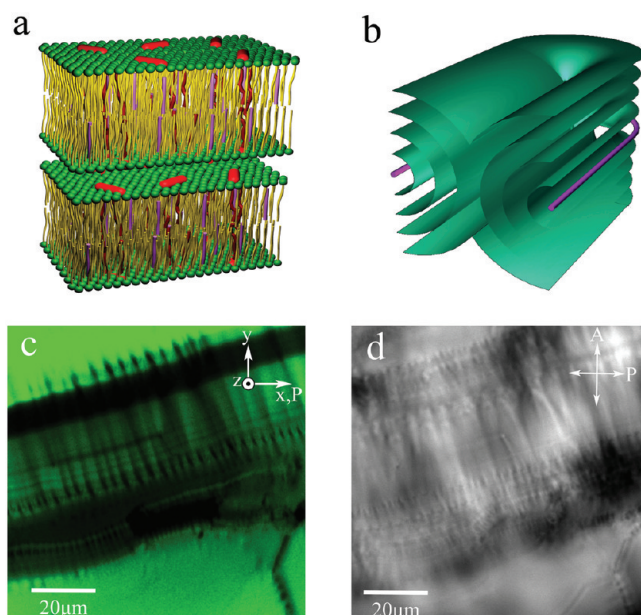
Figure 5. FCPM and PM imaging of layered structures, defects, and $\mathbf{n}(\mathbf{r})$ of the lyotropic lamellar LC. (a) A schematic of the self-assembly of the amphiphilic $DiOC_{18}(3)$ dye molecules into the flat bilayers of the lamellar lyotropic LC phase and their alignment with transition dipole moments parallel to the planes of layers. (b) A schematic of an oily streak defect of the lamellar LC. (c, d) Images of oily streak defects simultaneously obtained by use of (c) FCPM with $DiOC_{18}(3)$ as a fluorescent probe and (d) PM. The polarization of FCPM probing light is marked by "**P**" in (c). The crossed polarizer "**P**" and analyzer "**A**" are marked in (d).

bright regions of the fluorescence textures corresponding to the FCPM linear polarization of probing light **P** being orthogonal to $\mathbf{n}(\mathbf{r})$ and parallel to the disk-shaped micelles while the dark regions correspond to **P** parallel or at a small angle to $\mathbf{n}(\mathbf{r})$ (orthogonal to the micelles). In certain parts of the sample, the cholesteric layers have in-plane alignment (Figure 3a,b), as schematically in Figure 3c. However, there are also regions vertical, tilted, and strongly curved layers (Figure 3d,e). Dislocations and various types of disclinations are ubiquitous in this system and clearly visualized in 3D by use of the FCPM imaging with this amphiphilic dye. This example of imaging shows that our approach can be applied to chiral mesophases.

Interestingly, 3D imaging reveals that dislocations of large Burgers vector are common in the lyotropic cholesterics (Figure 3b,e), although they are rare in the thermotropic cholesteric LCs (in which, typically, only dislocations of Burgers vector equal to $p/2$ or p are observed).[33] Although the untreated surfaces of glass substrates impose tangential boundary conditions for $\mathbf{n}(\mathbf{r})$ and cholesteric layers, the layered structures are typically complex and nonuniform. These experimental findings are a likely consequence of the fact that lyotropic cholesterics have Frank elastic constants (including the twist elastic constant K_{22}) of about 1 pN, about an order of magnitude lower than their thermotropic counterparts.[33] In the sample regions with defects, the cholesteric layer spacing often departs from the equilibrium thickness $p/2$ of the elementary cholesteric lamella (Figure 3). This is, again, a natural result considering that the cholesteric layer compressibility modulus $B = K_{22}(2\pi/p)^2$ is at least an order of magnitude lower than that in the thermotropic cholesterics studied previously.[33] Furthermore, the obtained FCPM images

show that the dislocation cores in lyotropic cholesterics do not exhibit a tendency to split into the so-called λ-disclinations with nonsingular cores [with $\mathbf{n}(\mathbf{r})$ in the core parallel to the defect line]. On the contrary, the so-called τ-disclinations with $\mathbf{n}(\mathbf{r})$ in the core orthogonal to the defect line are equally frequently observed (Figure 3). In addition to the reasons related to the elastic energy costs of the defects, this difference compared to thermotropic cholesterics is caused by the fact that cores of τ-disclinations in lyotropic LCs do not have to melt to the isotropic phase (like in thermotropic LCs) but rather can be comprised of micelle-deprived water-rich regions, which likely reduces the core energy term of the overall free energy cost of these defects and makes them more abundant.

Figure 4 shows FCPM imaging of a lyotropic columnar hexagonal LC that, in addition to long-range orientational ordering, possesses the long-range two-dimensional positional ordering of the constituent building blocks (micelles). The used sample contains the so-called developable domains, the most typical defects in the columnar hexagonal LCs. Dye molecules of $DiOC_{18}(3)$ are again used as a fluorescent probes and align along the SDS/1-decanol cylindrical micelles and $\mathbf{n}(\mathbf{r})$ of this phase (Figure 4a). Since the bend-type distortions of $\mathbf{n}(\mathbf{r})$ in this phase are compatible with the hexagonal arrangement of micelles in the phase, they are not costly in terms of elastic energy and commonly observed (Figure 4c,d). These bend distortions of $\mathbf{n}(\mathbf{r})$ form the basis of the developable domain structure within which the two-dimensional translationally periodic hexagonal ordering of the micelles in the plane perpendicular to them is not disrupted (Figure 4b). FCPM imaging readily reveals the basic structure of the developable domains (Figure 4c), which is consistent with that obtained by use of polarizing optical microscopy (Figure 4d).

In the lamellar LC phase, the alignment of the used amphiphilic dye molecules with the absorption and fluorescence transition dipole moments parallel to the flat bilayers formed by surfactant molecules allows for the visualization of $\mathbf{n}(\mathbf{r})$, layered structures, and defects in this phase (Figure 5a,b). To illustrate this, we image the curvature defects in the system of parallel lamellae, the so-called "oily streaks" (Figure 5c,d). The bright regions of the polarized fluorescence textures correspond to lamellae parallel to **P** in the FCPM setup, and the dark regions correspond to lamellae orthogonal or oriented at large angles with respect to **P**. The patterns of $\mathbf{n}(\mathbf{r})$ and bilayer orientations in the oily streaks visualized by FCPM (Figure 5c) are in good agreement with the textures obtained by polarizing optical microscopy (Figure 5d) and a general schematic shown in Figure 5b. This example of visualization of $\mathbf{n}(\mathbf{r})$ in the lamellar phase with quasi-long-range one-dimensional positional ordering (along with the previous example of columnar hexagonal LC with two-dimensional long-range positional ordering) demonstrates that our approach enables 3D imaging of director fields not only in 3D nematic fluids but also in mesophases with various degrees of partial translational positional ordering.

4. CONCLUSIONS

We have demonstrated self-alignment of amphiphilic dye molecules within the building blocks of surfactant-based lyotropic liquid crystals that include oblate and prolate micelles and lamellae. This self-alignment enables 3D visualization of the director fields and defects of lyotropic LCs composed of cylindrical micelles and lamellae by use of fluorescence confocal polarizing microscopy and two-photon excitation fluorescence

polarizing microscopy. This approach can be further extended to imaging of lyotropic LCs composed of biaxial micelles, undulating bilayers, as well as to studying the features of orientational ordering in uniaxial and biaxial nematic phases, ripple phases, etc.[29,34,35] 3D imaging of lyotropic surfactant-based LCs with similar molecular labeling can be also further extended to the use of various other nonlinear optical microscopy techniques, including coherent anti-Stokes Raman scattering polarizing microscopy,[18,36] multiphoton excitation fluorescence and multiple harmonic generation microscopies,[16,17,37] and multimodal nonlinear optical polarizing microscopy.[18,38] The nonlinear optical microscopy based on stimulated Raman scattering[39] and several new techniques enabling subdiffraction-limited high-resolution optical imaging (see, for example, refs 40 and 41) can be extended to the use for purposes of orientation-sensitive imaging as well. The demonstrated capability of 3D imaging of orientational ordering in these lyotropic mesophases will further expand their utility in optical, photonic, biodetection,[3] templating, and other applications[11] and enhance our fundamental understanding of these intriguing soft matter systems.

■ AUTHOR INFORMATION

Corresponding Author
*Tel: 1-303-492-7277. Fax: 1-303-492-2998. E-mail: ivan.smalyukh@colorado.edu.

■ ACKNOWLEDGMENT

■ REFERENCES

(1) Chaikin, P. M.; Lubensky, T. C. *Principles of Condensed Matter Physics*; Cambridge University Press: Cambridge, 2000.

(2) de Gennes, P. G.; Prost, J. *The Physics of Liquid Crystals*; Oxford University Press: New York, 1995.

(3) Woltman, S. J.; Jay, D. G.; Crawford, G. P. *Nature Mater.* **2007**, *6*, 929–938.

(4) Oosten, C. L.; van Bastiaansen, C. W. M.; Broer, D. J. *Nature Mater.* **2009**, *8*, 677–682.

(5) Livolant, F.; Bouligand, Y. *Chromosoma* **1980**, *80*, 97–118.

(6) Poulin, P.; Stark, H.; Lubensky, T. C.; Weitz, D. A. *Science* **1997**, *275*, 1770–1773.

(7) Stark, H. *Phys. Rep.* **2001**, *351*, 387–474.

(8) Lubensky, T. C.; Pettey, D.; Currier, N.; Stark, H. *Phys. Rev. E* **1998**, *57*, 610–625.

(9) Loudet, J. C.; Poulin, P. *Phys. Rev. Lett.* **2001**, *87*, 165503.

(10) Loudet, J. C.; Barois, P.; Poulin, P. *Nature* **2000**, *407*, 611–613.

(11) Hoffmann, F.; Cornelius, M.; Morell, J.; Fröba, M. *Angew. Chem., Int. Ed.* **2006**, *45*, 3216–3251.

(12) (a) Liu, Q.; Cui, Y.; Gardner, D.; Li, X.; He, S.; Smalyukh, I. I. *Nano Lett.* **2010**, *10*, 1347–1353. (b) Mondiot, F.; Prathap Chandran, S.; Mondain-Monval, O.; Loudet, J.-C. *Phys. Rev. Lett.* **2009**, *103*, 238303.

(13) (a) Webb, R. H. *Rep. Prog. Phys.* **1996**, *59*, 427. (b) Pawley, J. B., Ed. *Handbook of Biological Confocal Microscopy*; Plenum Press: New York, 1995. (c) Zipfel, W. R.; Williams, R. M.; Webb, W. W. *Nature Biotechnol.* **2003**, *21*, 1369–1377. (d) Carriles, R.; Schafer, D. N.; Sheetz, K. E.; Field, J. J.; Cisek, R.; Barzda, V.; Sylvester, A. W.; Squier, J. A. *Rev. Sci. Instrum.* **2009**, *80*, 081101.

(14) Smalyukh, I. I.; Shiyanovskii, S. V.; Lavrentovich, O. D. *Chem. Phys. Lett.* **2001**, *336*, 88–96.

(15) Matthias, H.; Kitzerow, H.-S. *Mol. Cryst. Liq. Cryst.* **2009**, *508*, 127–136.

(16) Pillai, R. S.; Oh-e, M.; Yokoyama, H.; Brakenhoff, C. J.; Muller, M. *Opt. Express* **2006**, *14*, 12976.

(17) Xie, A.; Higgins, D. A. *Appl. Phys. Lett.* **2004**, *84*, 4014.

(18) Lee, T.; Trivedi, R. P.; Smalyukh, I. I. *Opt. Lett.* **2010**, *35*, 3447–3449.

(19) Smalyukh, I. I.; Butler, J.; Shrout, J. D.; Parsek, M. R.; Wong, G. C. L. *Phys. Rev. E* **2008**, *78*, 030701(R).

(20) Salter, P. S.; Carbone, G.; Botcherby, E. J.; Wilson, T.; Elston, S. J.; Raynes, E. P. *Phys. Rev. Lett.* **2009**, *103*, 257803.

(21) Smalyukh, I. I.; Zribi, O. V.; Butler, J. C.; Lavrentovich, O. D.; Wong, G. C. L. *Phys. Rev. Lett.* **2006**, *96*, 177801.

(22) Lentz, B. R. *Chem. Phys. Lipids* **1989**, *50*, 171–190.

(23) Lentz, B. R. *Chem. Phys. Lipids* **1993**, *64*, 99–116.

(24) van Zandvoort, M. A. M. J.; Gerritsen, H. C.; van Ginkel, G.; Levine, Y. K.; Tarroni, R.; Zannoni, C. *J. Phys. Chem. B* **1997**, *101*, 4149–4154.

(25) Krishna, M. M. G.; Periasamy, N. *J. Fluoresc.* **1998**, *8*, 81–91.

(26) Krishna, M. M. G.; Periasamy, N. *Chem. Phys. Lett.* **1998**, *298*, 359–367.

(27) Krishna, M. M. G.; Periasamy, N. *Biochim. Biophys. Acta* **1999**, *1461*, 58–68.

(28) Yu, L. J.; Saupe, A. *J. Am. Chem. Soc.* **1980**, *102* (15), 4879–4883.

(29) Figueiredo Neto, A. M.; Salinas, S. R. A. *The Physics of Lyotropic Liquid Crystals*; Oxford University Press: Cambridge, 2005.

(30) Hendrikx, Y.; Charvolin, J.; Rawiso, M.; Liebert, L.; Holmes, M. C. *J. Phys. Chem.* **1983**, *87*, 3991–3999.

(31) Galerne, Y.; Figueiredo Neto, A. M.; Liebert, L. *J. Chem. Phys.* **1987**, *87*, 1851–1856.

(32) Hendrikx, Y.; Charvolin, J.; Rawiso, M. *Phys. Rev. B* **1986**, *33*, 3534–3537.

(33) Smalyukh, I. I.; Lavrentovich, O. D. *Phys. Rev. Lett.* **2003**, *90*, 085503.

(34) Fu, Y.; Wang, H.; Shi, R.; Cheng, J.-X. *Biophys. J.* **2007**, *92*, 3251.

(35) Yu, L. J.; Saupe, A. *Phys. Rev. Lett.* **1980**, *45*, 1000–1003.

(36) Kachynskii, A.; Kuzmin, A.; Prasad, P. N.; Smalyukh, I. I. *Appl. Phys. Lett.* **2007**, *91*, 151905.

(37) Yoshiki, K.; Hashimoto, M.; Araki, T. *Jpn. J. Appl. Phys.* **2005**, *44*, L1066.

(38) Trivedi, R. P.; Lee, T.; Bertness, K.; Smalyukh, I. I. *Opt. Express* **2010**, *18*, 27658–27669.

(39) Saar, B. G.; Freudiger, C. W.; Reichman, J.; Stanley, C. M.; Holtom, G. R.; Xie, X. S. *Science* **2010**, *330*, 1368–1370.

(40) Betzig, E.; Patterson, G. H.; Sougrat, R.; Lindwasser, O. W.; Olenych, S.; Bonifacino, J. S.; Davidson, M. W.; Lippincott-Schwartz, J.; Hess, H. F. *Science* **2006**, *313*, 1642–1645.

(41) Rust, M. J.; Bates, M.; Zhuang, X. *Nature Methods* **2006**, *3*, 793–796.